Cerebral Cortex, 2017; 1–15

doi: 10.1093/cercor/bhx306
Original Article

ORIGINAL ARTICLE

p140Cap Regulates GABAergic Synaptogenesis and Development of Hippocampal Inhibitory Circuits

Isabella Russo[1], Daniela Gavello[2,3], Elisabetta Menna[4,5], David Vandael[2,3], Carola Veglia[1], Noemi Morello[6], Irene Corradini[4,5], Elisa Focchi[4], Annalisa Alfieri[1], Costanza Angelini[1], Federico Tommaso Bianchi[1,7], Alessandro Morellato[1], Andrea Marcantoni[2,3], Marco Sassoè-Pognetto[6,8], Matteo Maria Ottaviani[6], Latefa Yekhlef[9], Maurizio Giustetto[6,8], Stefano Taverna[9], Valentina Carabelli[2,3], Michela Matteoli[4,5], Emilio Carbone[2,3], Emilia Turco[1] and Paola Defilippi[1]

[1]Department of Molecular Biotechnology and Health Sciences, University of Torino, 10126 Torino, Italy, [2]Department of Drug Science, University of Torino, 10126 Torino, Italy, [3]NIS Centre of Excellence, 10126 Torino, Italy, [4]Institute of Neuroscience, CNR, 20129 Milano, Italy, [5]Istituto Clinico Humanitas, IRCCS, 20089 Rozzano, Italy, [6]Department of Neuroscience, University of Torino, 10126 Torino, Italy, [7]Neuroscience Institute Cavalieri Ottolenghi, University of Torino, 10043 Orbassano, Italy, [8]National Institute of Neuroscience—Italy, 10126 Torino, Italy and [9]Division of Neuroscience, San Raffaele Scientific Institute, 20132 Milano, Italy

Address correspondence to Emilio Carbone. Email: emilio.carbone@unito.it; Paola Defilippi. Email: paola.defilippi@unito.it.

Abstract

The neuronal scaffold protein p140Cap was investigated during hippocampal network formation. p140Cap is present in presynaptic GABAergic terminals and its genetic depletion results in a marked alteration of inhibitory synaptic activity. p140Cap$^{-/-}$ cultured neurons display higher frequency of miniature inhibitory postsynaptic currents (mIPSCs) with no changes of their mean amplitude. Consistent with a potential presynaptic alteration of basal GABA release, p140Cap$^{-/-}$ neurons exhibit a larger synaptic vesicle readily releasable pool, without any variation of single $GABA_A$ receptor unitary currents and number of postsynaptic channels. Furthermore, p140Cap$^{-/-}$ neurons show a premature and enhanced network synchronization and appear more susceptible to 4-aminopyridine-induced seizures in vitro and to kainate-induced seizures in vivo. The hippocampus of p140Cap$^{-/-}$ mice showed a significant increase in the number of both inhibitory synapses and of parvalbumin- and somatostatin-expressing interneurons. Specific deletion of p140Cap in forebrain interneurons resulted in increased susceptibility to in vitro epileptic events and increased inhibitory synaptogenesis, comparable to those observed in p140Cap$^{-/-}$ mice. Altogether, our data demonstrate that p140Cap finely tunes inhibitory synaptogenesis and GABAergic neurotransmission, thus regulating the establishment and maintenance of the proper hippocampal excitatory/inhibitory balance.

Key words: p140Cap, GABAergic synaptogenesis, GABAergic neuron development, GABAergic neurotransmission

Introduction

Synaptic excitation/inhibition (E/I) balance is crucial for brain function (Hensch 2005; Maffei et al. 2006; Yizhar et al. 2011) and its alteration underlies several neurological conditions. The comprehension of the cellular mechanisms that regulate E/I balance is therefore crucial to understand brain development and functioning in order to discover new molecular bases of brain diseases. A wide range of developmental and physiological mechanisms has been identified that maintain the E/I equilibrium (Englot et al. 2009; Tatti et al. 2017). Inhibitory interneurons (INs) are key participants in the generation of normal neural activity in the cerebral cortex and hippocampus. By innervating selectively different domains of pyramidal cells, they are the main source of "feedback" and "feed-forward" inhibition (Kullmann 2011). GABAergic INs critically pace and synchronize populations of excitatory principal cells to coordinate neuronal information processing (McBain and Fisahn 2001; Klausberger and Somogyi 2008).

In line with INs playing a central role in the control of neural activity, GABAergic deficits lead to pathological conditions and contribute to cognitive deficits associated with several psychiatric and neurological diseases. Recent studies have highlighted that alterations in the inhibitory network are involved in dysfunctions associated with schizophrenia, autism and intellectual disabilities (Coghlan et al. 2012; Marín 2012). In addition, selective enhancement of GABAergic synaptogenesis has been found to induce a permanent increase in the inhibitory tone throughout the brain, reduced synaptic plasticity in the hippocampus, and severe forms of intellectual disability (Papale et al. 2017).

p140Cap is an adapter protein highly expressed in neurons, encoded by the SRCIN1 gene, initially identified as a SNAP25-binding protein (Chin et al. 2000) and as a key element of the postsynaptic density (Ito et al. 2008). Indeed, p140Cap localizes to dendritic spines and its down-regulation in hippocampal excitatory neurons negatively affects their morphology and synaptic plasticity via regulation of the microtubule cytoskeleton (Jaworski et al. 2009). In agreement, p140Cap$^{-/-}$ mice show defects in learning and memory, a decreased long-term potentiation (LTP) and long-term depression (LTD), and extensive remodeling of the actin cytoskeletal architecture of synapses (Repetto et al. 2014). In addition, p140Cap interacts with proteins essential for transmission across chemical synapses (both excitatory and inhibitory synapses) and cell-cell junctions (Alfieri et al. 2017), enlightening a key role in synaptogenesis, synaptic transmission and synaptic plasticity.

In this work, we show that p140Cap is present in the inhibitory presynaptic compartment. Genetic ablation of p140Cap from neurons leads to enhanced frequency of miniature inhibitory postsynaptic currents (mIPSCs), increased size of electrically evoked inhibitory postsynaptic currents (eIPSCs) and early synchronization of hippocampal network, with significantly higher firing activity. Surprisingly, p140Cap$^{-/-}$ mice display an enhanced susceptibility to the pharmacological induction of epileptic seizures combined with an increased density of INS and inhibitory GABAergic synapses. Conditional mice lacking p140Cap specifically in forebrain INs display an increase of both susceptibility to in vitro epileptic events and density of inhibitory synapses, comparable with null mice. Together, these data highlight a crucial role of p140Cap in inhibitory network development and maturation.

Materials and Methods

Mice and Treatments

p140Cap$^{-/-}$ mice were previously described (Repetto et al. 2014). Mice were maintained in the transgenic unit of the Molecular Biotechnology Center (University of Turin, Turin, Italy) and provided with food and water ad libitum. Genetic screening was performed by PCR as previously described (Repetto et al. 2014). To obtain a p140Cap floxed allele, we designed the targeting construct as follows: both the fifth exon and the 11th exon of p140Cap gene were flanked with loxP sites, the second one bearing also the neomycin resistance gene, flanked with Flippase Recognition Target (FRT) sites to permit its excision (See Supplementary Fig. S2). This construct was introduced by electroporation into mouse ES cells and homologous recombination was confirmed by Southern blot. ES cells carrying p140Cap-fl-neo allele were injected into C57 blastocysts to generate germ-line chimeras. The neomycin resistance cassette in the targeting construct was removed by crossing heterozygous p140Cap + /fl-neo mice with mice carrying the FLP recombinase under the control of the actin promoter (from The Jackson Laboratory) to produce mice carrying the p140Cap floxed allele. To generate interneuron specific p140Cap knockout mice, p140Cap fl/fl mice were crossed to mice expressing the Cre recombinase under the control of the Dlx5/6 promoter (from The Jackson Laboratory) to obtain p140Cap fl/fl;Dlx5/6-Cre mice. Animal care and handling throughout the experimental procedures were conducted in accordance with European Community Council Directive 2010/63/UE for care and use of experimental animals and were approved by the Italian Ministry of Health (Authorization 49/2014-PR) and by the Bioethical Committee of the University of Turin. All efforts were made to minimize animal suffering and to reduce the number of animals used.

Cultured Neurons on MEAs

Hippocampal neurons were obtained from WT and p140Cap$^{-/-}$ 18-day embryos. Hippocampus was rapidly dissected under sterile conditions, kept in cold HBSS (4 °C) with high glucose, and then digested with papain (0,5 mg/ml) dissolved in HBSS plus DNAse (0,1 mg/ml) (Trygve et al. 2007; Gavello et al. 2012). Isolated cells were then plated at the final density of 1200 cells/mm^2 onto the MEA (previously coated with poly-DL-lysine and laminin) and allowed to adhere on the center of the chip by using a ring made of Sylgard 184 (Dow Corning), 4.5 mm internal diameter (11 mm external diameter), which was removed after 4 h. The cells were incubated with 1% penicillin/streptomycin, 1% glutamax, 2.5% fetal bovine serum, 2% B-27 supplemented neurobasal medium in a humidified 5% CO2 atmosphere at 37 °C. Each MEA dish was covered with a fluorinated ethylene-propylene membrane (ALA scientific, Westbury, NY, USA) to reduce medium evaporation and maintain sterility, thus allowing repeated recordings from the same chip. Recordings were carried out since 11 Days in Vitro (DIV) until DIV 18. Culture medium was partially (1/3) changed once a week, depending on the age of the culture (young cultures did not need weekly change of medium). Following experiments, MEA dishes were re-used by cleaning overnight in 1% Tergazyme (Sigma-Aldrich, St. Louis, MO), rinsing in distilled water and then sterilizing overnight under UV ray.

MEA Recordings

Multisite extracellular recordings were performed using the MEA-system, purchased from Multi-Channel Systems (Reutlingen, Germany). The 60 electrodes array (TiN/SiN) is composed by a 8 × 8 square grid with 200 μm inter-electrode spacing and 30 μm electrode diameter. Data acquisition was controlled through MC_Rack software (Multi-Channel Systems Reutlingen, Germany), setting the threshold for spike detection at −15 μV and sampling at 10 kHz. Experiments were performed in a non-humidified incubator at 37 °C and with 5% CO2, without replacing the culture medium. Before starting the experiments, cells were allowed to stabilize in the non-humidified incubator for 90 s; recording of the spontaneous activity was then carried out for 90 s.

Analysis of MEA Activity

Burst analysis was performed using Neuroexplorer software (Nex Technologies, Littleton, MA, USA) after spike sorting operations. Because a burst consists of a group of spikes with decreasing amplitude (Vaghi et al., 2014), we set a threshold of at least 3 spikes and a minimum burst duration of 10 ms. We set interval algorithm specifications such as maximum interval to start burst (0.17 s) and maximum interval to end burst (0.3 s) recorded in 0.02 s bins. Burst analysis has been performed by monitoring the following parameters: number of spikes, frequency, number of bursts and burst duration. Cross-correlation probability versus time diagrams were constructed by means of Neuroexplorer software (Nex Technologies, Littleton, MA, USA), using ±0.5 s and ±3.5 s and 5 ms bin size. Data are expressed as means ± S.E.M and statistical significance was calculated by using Student's unpaired *t*-test. Values of $P < 0.05$ were considered significant.

Electrophysiological Recordings and Data Analysis in Cultured Neurons

Patch electrodes, fabricated from thick borosilicate glasses (Hilgenberg, Mansfield, Germany), were pulled and fire-polished to a final resistance of 2–4 MΩ. Patch clamp recordings were performed in whole-cell configuration using a Multiclamp 700-B amplifier connected to a Digidata 1440 and governed by the pClamp10 software (Axon Instruments, Molecular Devices Ltd., USA) (Marcantoni et al. 2009, 2014). mIPSCs and eIPSCs were acquired at 1–10 kHz sample frequency and filtered at one-half the acquisition rate with an 8-pole low-pass Bessel filter (Baldelli et al. 2005). Recordings with leak currents of >100 pA or a series resistance of >20 MΩ were discarded. All the experiments were performed at room temperature (22–24 °C).

Peak-scaled variance analysis - Analysis of mIPSCs was performed as described by (Baldelli et al. 2005), using MiniAnalysis programs (version 6.0.3, Synaptosoft, Leonia, NJ) and following the signal analysis requirements discussed in (Traynelis et al. 1993). The variance analysis of mIPSCs was used to determine the number of GABA receptor channels (N_{Ch}) and their mean unitary current (i) (Fig. 2A). Briefly, 60 to 130 mIPSCs were selected and averaged. The mean waveform obtained from the average of N trace was scaled to the peak of each individual mIPSC and subtracted. The mean variance $\sigma^2(t)$ was then calculated by summing the squares of the difference traces divided by N-1 and plotted versus the decaying phase of mean current I(t) (gray area in Fig. 2A).

Evoked IPSCs (eIPSCs)—Monosynaptic GABAergic eIPSCs were recorded following the approach described in (Baldelli et al. 2005). Current pulses of 0.1 ms and variable amplitude (8–30 μA) were generated by an isolated pulse stimulator (model 2100; A-M-System, Carlsburg, WA) and delivered through a glass pipette of 1 μm tip diameter filled with Tyrode's solution placed in contact with the cell body of the GABAergic IN in a loose-seal configuration (Baldelli et al. 2005). The postsynaptic neuron was voltage-clamped and maintained at a holding potential of −70 mV. The current artifact produced by the presynaptic extracellular stimulation was subtracted in the eIPSCs shown.

Solutions and Drugs

mIPSCs were recorded by superfusing the whole-cell-clamped postsynaptic neuron with Tyrode's solution containing (in mM): 2 $CaCl_2$, 150 NaCl, 1 $MgCl_2$, 10 HEPES, 4 KCl, and 10 glucose, pH 7.4 (Baldelli et al. 2005). When required, solutions with higher Ca^{2+} concentrations (5–10 mM) were prepared by lowering the NaCl content. The unselective glutamate receptor antagonist, kynurenic acid (1 mM) (Sigma), was added to the Tyrode's solution to block excitatory transmission. Tetrodotoxin (0.3 μM) was added to block spontaneous action potential propagation. The neuron was constantly superfused through a gravity system, as previously described (Baldelli et al. 2005). The perfusion solution was changed rapidly (50–60 ms) and applied for variable periods of time. The tip of the perfusion pipette (100–200 μm) was placed 40–80 μm to the cell body. The standard internal solution was (in mM): 90 CsCl, 20 TEA-Cl, 10 EGTA, 10 glucose, 1 $MgCl_2$, 4 ATP, 0.5 GTP, and 15 phosphocreatine, pH 7.4. K+ was substituted for Cs+ and TEA+ in the pipette solution to block outward potassium currents. N-(2,6-dimethylphenylcarbamoylmethyl) triethylammonium bromide (10 mM) was added to block Na^+ currents activated during an eIPSC (Baldelli et al. 2005). The hypertonic sucrose containing solution was prepared by adding 500 mM sucrose to the Tyrode.

Slice Electrophysiology

Mice of both sexes (34–40 days of age) were anesthetized with an intraperitoneal injection of a mixture of ketamine/xylazine (100 mg/kg and 10 mg/kg, respectively) and perfused transcardially with ice-cold artificial cerebrospinal fluid (ACF) containing (in mM): 125 NaCl, 3.5 KCl, 1.25 NaH_2PO_4, 2 $CaCl_2$, 25 $NaHCO_3$, 1 $MgCl_2$, and 11 D-glucose, saturated with 95% O_2 5% CO_2 (pH 7.3). After decapitation, brains were removed from the skull and 300 μm-thick horizontal slices containing the entorhinal cortex and the hippocampus were cut in ACF at 4 °C using a VT1000S vibratome (Leica Microsystems, Wetzlar, Germany). Individual slices were then submerged in a recording chamber mounted on the stage of an upright BX51WI microscope (Olympus, Japan). Slices were perfused with ACF continuously flowing at a rate of 2–3 ml/min at 32 °C. Glass electrodes (tip resistance 1–2 MΩ) were filled with ACF and positioned in the CA1 area of the hippocampus and layer II–III of the medial entorhinal cortex (mEC), ~250 μm below the pial surface. Local field potentials (LFP) were acquired at a frequency of 10 kHz and band-passed within a 1 Hz–1 kHz frequency range. All recordings were performed using a MultiClamp 700B amplifier interfaced with a PC through a Digidata 1440 A (Molecular Devices, Sunnyvale, CA, USA). Data were acquired using pClamp10 software (Molecular Devices) and analyzed with Origin 9.1 (Origin Lab, Northampton, MA, USA).

Kainate-induced Seizures

Susceptibility to kainate-induced seizures was determined as previously described (Bozzi et al. 2000; Corradini et al. 2014). Briefly, p140Cap$^{+/+}$, p140Cap$^{-/-}$, Flox-p140Cap and C-p140Cap mice received 25–35 mg/kg body weight intraperitoneal (i.p.) kainic acid (KA, Sigma Aldrich, St. Louis, MO) dissolved in saline solution. Following injection, animals were returned to cages where seizure severity was scored every 10 min for a maximum of 3 h, according to a modified Racine scale (Bozzi et al. 2000; Corradini et al. 2014): stage 0, normal behavior; stage 1, immobility; stage 2, forelimb and/or tail extension, rigid posture; stage 3, repetitive movements, head bobbing; stage 4, rearing and falling; stage 5, continuous rearing and falling; stage 6, severe whole-body convulsions; stage 7, death. Saline-injected animals of both genotypes were used as controls. Observers were blind to treatment and genotype of each animal and scores were assigned based on the maximum stage reached during the observational period. Data collected were used to calculate the time course of seizure severity for each genotype.

Immunofluorescence on Primary Hippocampal Cultures

Primary hippocampal cultures were fixed at 16 DIV with 4% formaldehyde 4% sucrose, and immunofluorescence staining was performed using the following antibodies: p140Cap monoclonal antibody (generated in our lab and used 1:500) and VGAT Rabbit polyclonal (affinity purified from Synaptic System 131 003, 1:500). After 3 washings in phosphate-buffer saline (PBS), cultured neurons were rinsed in a PBS—0.1% Triton solution for 5 min followed by 30 min of saturation with PBS—5% BSA at room temperature. The primary antibody was diluted in a PBS—1% BSA solution and incubated for 2–3 h at 4 °C. After 3 washes, secondary antibodies were incubated at 1:1000 for 1 h at R.T. Coverslips were mounted with Prolong. Images were acquired at LSM 510 META confocal microscope (Leica Microsystems, Germany), using a 63×-oil objective and analyzed with Fiji ImageJ software.

Immunohistochemistry and Immunofluorescence

For immunohistochemistry experiments, animals were anesthetized with an intraperitoneal injection of a mixture of Zoletil (fixed-ratio combination 1:1 of zolazepam and tiletamine) (Zoletil: 80 mg/Kg. Alcyon, Italy) and Xilazine (Nerfasin: 10 mg/Kg. Alcyon, Italy) and transcardially perfused with PBS followed by 4% ice-cold formaldehyde in 0.1 M phosphate buffer (PB, pH 7.4). After perfusion, brains were dissected and postfixed in the same fixative solution overnight at 4 °C. After several washes in 0.1 M PB, brains were cryoprotected by immersion in 10, 20, and 30% sucrose solutions. Coronal sections (30 µm) were cut with a cryostat and stored at 20 °C in a solution containing 30% ethylene glycol and 25% glycerol in 0.1 M PB (pH 7.2) until processing. Immunohistochemistry was carried out according to a protocol for free-floating sections as previously described (Morello et al. 2017). After being rinsed in PBS (3 × 10 min), sections were immersed in 1% H_2O_2 in PBS for 20 min to block endogenous peroxidase activity. After a blocking step in PBS containing 0.05% Triton X-100 and 10% normal goat serum (NGS), sections were incubated overnight at RT with the following primary antibodies diluted in PBS with 3% NGS and 0.05% Triton X-100: rat anti-somatostatin (SOM, MAB354, 1:250; Millipore Corporation), rabbit anti-calretinin (CR, 214 102, 1:500; SYSY, Goettingen, Germany), mouse anti-parvalbumin (PV, 235, 1:10 000; Swant, Marly, Switzerland). The following day, after several PBS rinses, the sections were incubated for 1 h with the appropriate biotinylated secondary antibodies (1:250, Vector Labs; Burlingame, CA) diluted in PBS with 3% NGS and 0.05% Triton X-100, followed by 1 h incubation in a solution containing a biotin-avidin complex (1:100, Vector Labs). Finally, sections were immersed in a solution containing 3,3′-diaminobenzidine (DAB) (0.05% in TRIS-HCl, pH 7.6) with 0.01% H_2O_2 as chromogen for the peroxidase reaction.

For immunofluorescence experiments, following 3 rinses in PBS and the blocking step, sections were incubated overnight at 4 °C with the following primary antibodies: rabbit polyclonal anti-VGAT (VGAT, 131 003, 1:1000 SYSY) and mouse monoclonal anti-neuron-specific nuclear protein (NeuN, MAB377 clone A60, 1:500, Merck Millipore). On the following day, after 3 washing in PBS, sections were immersed for 2 h at RT in secondary fluorescent antibodies (Alexa Fluor Secondary Antibodies 1:200, Invitrogen). After several PBS rinses, the sections were mounted on glass slides and observed with a bright-field microscope (Eclipse 800, Nikon, Japan) equipped with a CCD camera (Axiocam HRc, Zeiss, Germany) or a 510 META laser-scanning confocal microscope (Zeiss, Germany).

Quantitative Analysis of Immunohistochemical Signals

The numbers of INs were estimated in coronal sections. For each animal, 4 sections along the rostro-caudal axis of the dorsal hippocampus were analyzed. Digital micrographs were processed with the software ImageJ, and the number of immunolabeled cells was calculated manually. All data are reported as mean ± SEM. Statistical analysis was done by Student's *t*-test, using GraphPad Prism software (La Jolla, CA, USA). For the quantification of inhibitory synapses, images were acquired in stratum pyramidale of the CA1 hippocampal subfield using a 40× oil immersion lens with an additional confocal zoom of up to 3 (voxel sizes of 0.10 × 0.10 × 1 µm). The parameters of acquisition (laser power, pinhole, gain, offset) were maintained constant between the 2 groups. Images were analyzed with the ImageJ software.

Electron Microscopy

Mice were perfused with 1% formaldehyde/1% glutaraldehyde in phosphate buffer (0.1 M PB, pH 7.4). Their brains were postfixed in the same fixative overnight, and small specimens taken from the dorsal hippocampus were postfixed in 1% OsO_4 in 0.1 M cacodylate buffer, dehydrated, and embedded in epoxy resin. Ultrathin sections were stained with uranyl acetate and lead citrate and observed in a JEM-1010 transmission electron microscope (Jeol) equipped with a side-mounted CCD camera (Mega View III, Soft Imaging System). The density of perisomatic GABAergic synapses was assessed by analyzing 381 digitized images from 3 p140Cap$^{-/-}$ and 3 control mice. Images were captured in CA1 stratum pyramidale. Type 2 synapses surrounding the cell body of pyramidal neurons were identified by the presence of numerous presynaptic vesicles, a visible synaptic cleft and symmetric pre- and postsynaptic specializations. The perimeter of pyramidal cells was measured with the Mega View software. Image acquisition and morphometric analysis were performed by an experimenter blind to the genotype of the mice.

Real-time PCR

Total RNA was extracted from dissected Median Ganglionic Eminence (MGE), Caudal Ganglionic Eminence (CGE) and

Lateral Ganglionic Eminence (LGE) samples from E15.15 p140Cap$^{+/+}$ embryos using Trizol Reagent (Ambion, Life Technologies Italia, Torino, Italy) and its concentration was determined with a NanoDrop™ 1100 (NanoDrop Technologies, Wilmington, DE, USA). Total RNA was reverse-transcribed with a high capacity cDNA reverse transcription kit (#4 368 813, Applied BioSystem) according to manufacturer's instruction and amplified with specific primers. RT-PCR analysis was carried out in 96-well plates in the ABI Prism 7300 real-time PCR system using Power SYBR® Green PCR Master Mix (#4 367 659, Invitrogen), specific primers and 10 ng total RNA converted into cDNA in 10 µl final volume.

Primers sequences:

p140Cap FW 5′CGGGATCCTGCAGCGGCAGCGCAC3′
p140Cap REV 5′GCGAATTCCACATACCCTCATCCACTTGCC3′
GAPDH FW 5′AGAAGGTGGTGAAGCAGGCATC3′
GAPDH REV 5′CGGCATCGAAGGTGGAAGAGTG3′

Immunostaining of Mouse Embryonic Cortex

Embryonic brains were dissected at E12.5 and fixed for 12–16 h at 4 °C in 4% formaldehyde. To evaluate proliferation, pregnant females were injected at E12.5 with 35 mg/kg 5-ethynyl-2 deoxyuridine (EdU). Fixed brains were equilibrated in 30% sucrose in PBS for 12–24 h at 4 °C, embedded with Tissue-TEK (O.C.T., Sakura Finetek), snap-frozen in liquid nitrogen, and stored at –20 °C. Sectioning was performed at 20 µm with a cryostat. Cryosections were rehydrated 5 times in PBS before further processing. For Nkx2.1 staining, monoclonal antibodies 8G7G3/1 from Thermo fisher were used at 1:100 dilution. Cryosections were subjected to antigen retrieval by heating in 0.01 M citrate buffer pH 6.0 at 70 °C for 1 h. Sections were permeabilized using 0.3% Triton X-100 in PBS for 30 min and quenched with 0.1 M glycine for 30 min, and incubated with primary antibodies overnight at 4 °C, followed by secondary antibody for 1 h at room temperature in a solution of 0.2% gelatin, 300 mM NaCl, and 0.3% Triton X-100 in PBS. DNA was stained in the last wash using DAPI. For EdU detection, the Click-iT EdU Alexa Fluor 488 Imaging Kit (Invitrogen, Carlsbad, CA) was used, according to the supplier's instructions. Apoptosis was measured by the TUNEL assay using "In Situ cell death detection kit, TMD red" (Roche, Basel; Switzerland) according to manufacturer's protocol. Following TUNEL staining, sections were counterstained with DAPI. The slides were mounted using ProLong anti-fade reagent (Thermo Fisher Scientific, Waltham, MA, USA). Imaging was performed using a Leica TCS SP5-AOBS 5-channel confocal system (Leica Microsystems) equipped with a 405-nm diode, an argon ion, and a 561-nm DPSS laser. Fixed cells were imaged using a HCX PL APO 20X/ DRY objective. Edu+ cells were counted on DAPI+ cells, from a cropped MGE image of known area, processed with ImageJ software.

Results

p140Cap Localizes at Inhibitory Synapses and its Loss Leads to Presynaptic GABAergic Alterations

We have previously demonstrated that p140Cap is part of the excitatory postsynaptic compartment (Jaworski et al. 2009; Repetto et al. 2014). To investigate if p140Cap localizes at inhibitory synapses, we performed double labeling immunofluorescence of primary hippocampal neurons using an antibody that recognizes the vesicular GABA transporter VGAT, a specific marker of inhibitory presynaptic terminals. The colocalization of p140Cap (green labeling) with VGAT (red labeling) was evident in 16 DIV cultures (Fig. 1A), suggesting presynaptic localization. This is consistent with previous electron microscopic observations in the rat brain (Ito et al. 2008).

To investigate the functional relevance of p140Cap at inhibitory synapses, we tested whether removal of p140Cap altered the synaptic activity of inhibitory INs. Miniature GABAergic post synaptic currents (mIPSCs) were recorded from 16-18 DIV hippocampal p140Cap$^{+/+}$ or p140Cap$^{-/-}$ neurons. Cells were held at –70 mV (V_h), and perfused locally with a Tyrode solution containing 300 nM TTX and 1 mM kynurenic acid to block both spontaneous action potentials and glutamatergic postsynaptic activity. Data were collected from 3 independent experiments for each genotype (Fig. 1B) (Baldelli et al. 2002, 2005; Allio et al. 2015). p140Cap ablation increased mIPSCs frequency by approximately 4-fold compared to controls. Mean inter-event intervals decreased from 1.74 ± 1.2 s in control (n = 1371 from 16 cells) to 0.33 ± 0.02 s in p140Cap$^{-/-}$ neurons (n = 1775 from 13 cells; $p < 0.001$) (Fig. 1C, left panel), with no difference in the average amplitude (–38.5 ± 0.9 pA in control vs. –40.1 ± 0.6 pA in p140Cap$^{-/-}$ neurons; $p = 0.135$) (Fig. 1D, left panel). The corresponding cumulative probability functions of the inter-event intervals and amplitudes are shown in Fig. 1C,D (right panels). These data are consistent with a potential presynaptic alteration of basal GABA release in the absence of p140Cap.

We then investigated whether p140Cap ablation altered the electrically evoked inhibitory postsynaptic currents (eIPSCs) induced by presynaptic action potential stimulation. The absence of the adapter protein caused a marked increase of eIPSCs (0.78 ± 0.12 nA in control (n = 14 cells) versus 1.32 ± 0.33 nA in p140Cap$^{-/-}$ neurons (n = 8 cells); $p = 0.033$) (Fig. 1E). To test if p140Cap$^{-/-}$ neurons exhibit a larger synaptic vesicle readily releasable pool (RRP), neurons were stimulated with a 500 mM hypertonic sucrose modified Tyrode's solution. The integral of the area under the current evoked by the stimulus that represents the RRP (Pyle et al. 2000) was significantly larger in p140Cap$^{-/-}$ neurons as compared to controls ($p = 0.023$, unpaired t-test) (Fig. 1F). The same occurred to the current amplitude that increased from –0.80 ± 0.09 nA in control (n = 14 cells) to –1.34 ± 0.28 nA in p140Cap$^{-/-}$ neurons (n = 8 cells) (p = 0.018, unpaired t-test). Conversely, the postsynaptic response of primary hippocampal neurons to saturating GABA concentrations (10 µM) was comparable in control and p140Cap$^{-/-}$ neurons ($p = 0.527$) (Fig. 1G).

Given that ablation of p140Cap does not alter the mean amplitude of miniature events in 16-18 DIV hippocampal neurons, it is likely that the absence of p140Cap preserves the unitary conductance and the density of postsynaptic $GABA_A$ receptors. To examine this, we measured the unitary conductance of $GABA_A$ channels by using the peak-scaled variance analysis (PSVA) of mIPSCs, which allows an estimate of the unitary current i carried by single postsynaptic $GABA_A$ channels (Traynelis et al. 1993). Figure 2A summarizes the procedure followed to determine the variance, $\sigma^2(t)$, from a group of mIPSCs, with data collected from 3 independent experiments for each genotype (see Materials and Methods). In 16-18 DIV neurons, loss of p140Cap caused almost no changes to the $\sigma^2(t)$ versus mean current (I(t)) relationship (Fig. 2B,C). The plot was clearly parabolic in both cases. The initial slope of the parabola yielded an estimate of the weighted single-channel current. On average, we obtained similar mean unitary currents of –2.2 ± 0.1 pA (n = 13 cells) and –2.0 ± 0.1 pA (n = 9 cells) in control and p140Cap$^{-/-}$ neurons ($P = 0.469$), respectively (Fig. 2D),

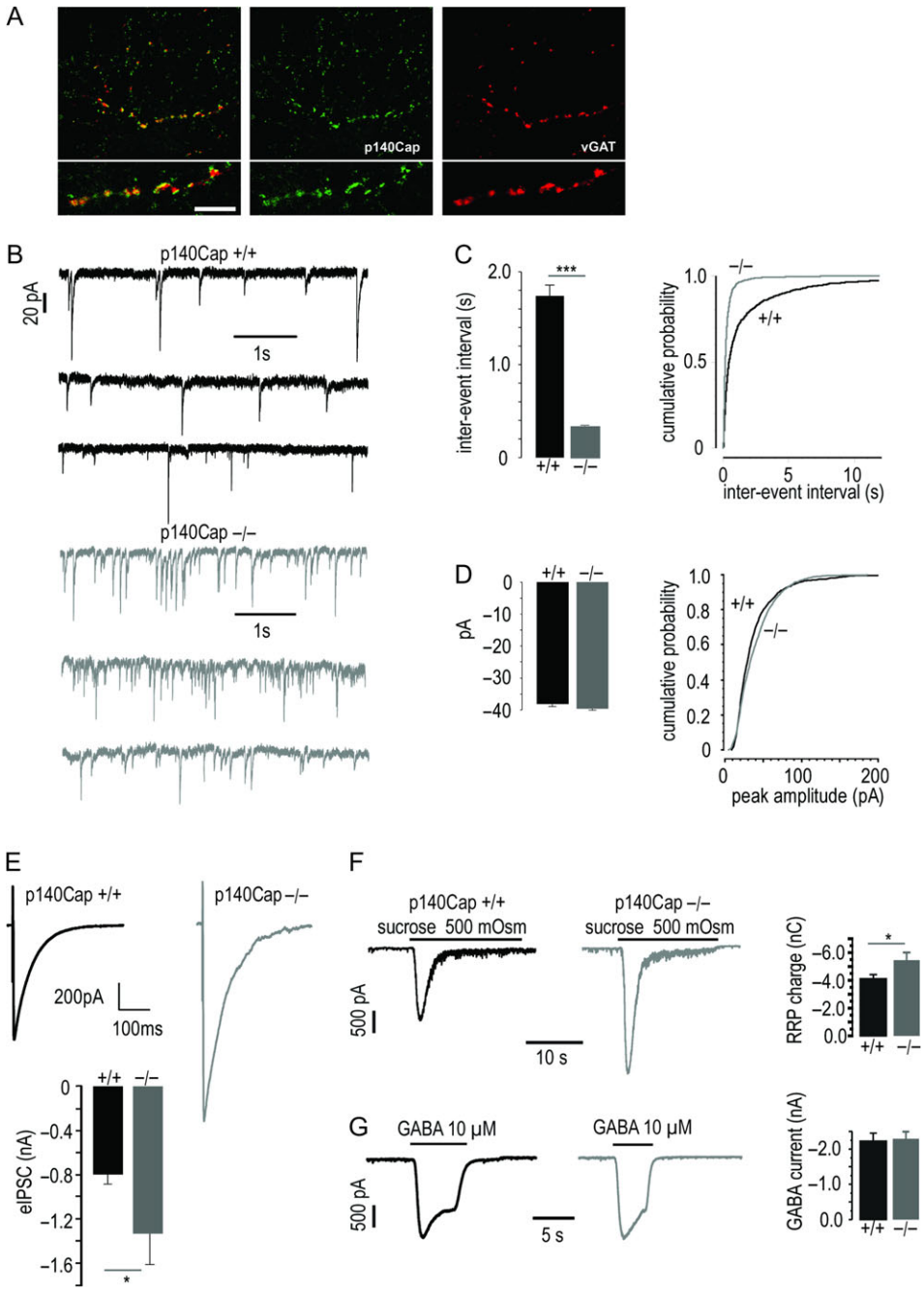

Figure 1. Localization of p140Cap in the VGAT-positive presynaptic compartment and presynaptic electrophysiological GABAergic alterations in p140Cap$^{-/-}$ mice. (*A*) p140Cap localizes with the inhibitory presynaptic marker VGAT// Immunofluorescence staining on 16 DIV hippocampal primary interneurons. Cells were stained for p140Cap in green and VGAT in red; scale bar: 10 µm. (*B*) Representative mIPSCs recorded from p140Cap$^{+/+}$ (black traces); and p140Cap$^{-/-}$ (gray traces) primary hippocampal cultures at 16-18 DIV. (*C*) Cumulative probability functions of the inter-event intervals for p140Cap$^{+/+}$ (black trace) and p140Cap$^{-/-}$ (gray trace). The inset to the left shows the mean frequency of events that results 4-fold higher for p140Cap$^{-/-}$ as compared to p140Cap$^{+/+}$. (*D*) Same as for (*C*) but concerning the mIPSC amplitude. (*E*) Top. Representative eIPSCs recorded during presynaptic stimulation of a control (black trace) and p140Cap$^{-/-}$ (gray trace) neurons; Vh = −70 mV. Bottom. The mean peak amplitude of eIPSCs from control and p140Cap$^{-/-}$ neurons. (*F*) Response of neurons to 500 mM hypertonic sucrose containing Tyrode's solution. (*G*) Representative postsynaptic responses of hippocampal neurons to 10 µM GABA. Black trace is from p140Cap$^{+/+}$ neurons while gray trace is from p140Cap$^{-/-}$ cells.

corresponding to a mean single-channel conductance of 31.0 and 28.6 pS. Because the mean amplitude of mIPSCs was not altered by the absence of p140Cap (Fig. 1*D*, left panel), we concluded that in 16-18 DIV hippocampal neurons the density of $GABA_A$ receptors was unaffected by the loss of p140 Cap (Fig. 1*D*, right panel).

Taken together, these data indicate that loss of p140Cap has specific potentiating presynaptic effects, consisting in enhanced RRP that result in increased mIPSC frequency and higher eIPSCs, without effects on the conductance and density of functional postsynaptic $GABA_A$ receptors. Interestingly, confocal analysis revealed a significant increase of the density of

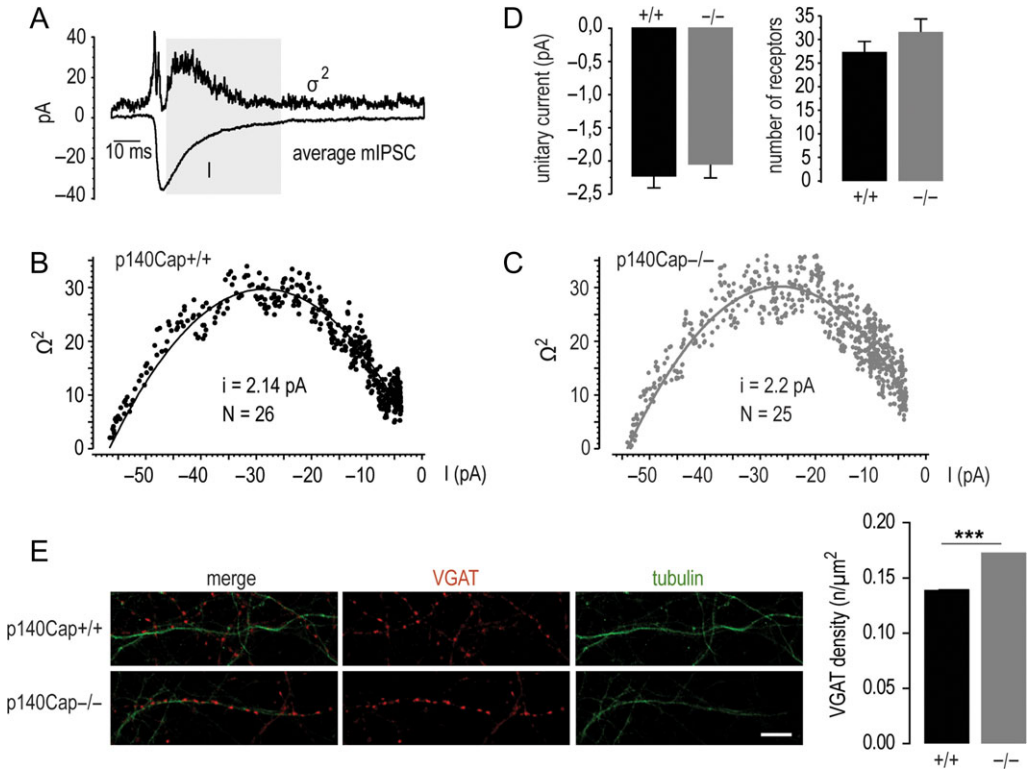

Figure 2. Peak-scaled variance analysis of mIPSCs and overall density of VGAT punctae. (*A–D*) Peak-scaled variance analysis of mIPSCs. (*A*) Time course of the mean variance σ^2(t) (top) and mean current I(t) (bottom), obtained by averaging mIPSCs of nearly the same amplitude. The gray rectangle indicates the temporal window where the σ^2 vs. I plots of panel (*B*) and (*C*) were derived (see Materials and Methods for details). (*B*,*C*) σ^2 vs. I plots obtained from mIPSCs recorded in p140Cap$^{+/+}$ (*B*) and p140Cap$^{-/-}$ neurons (*C*). (*E*) Representative images of 16-18 DIV p140Cap$^{+/+}$ and p140Cap$^{-/-}$ hippocampal primary neurons stained for the inhibitory presynaptic marker vGAT (red) and the microtubule protein Tubulin (green), and relative quantification of the density of VGAT puncta per unit length. Scale bar value = 10 µm.

VGAT puncta formed on target dendrites by individual axons in p140Cap$^{-/-}$ neurons, with respect to age-matched control neurons (Fig. 2*E*) (number of VGAT/µm, p140Cap$^{+/+}$ = 0.139 ± 0.006; p140Cap$^{-/-}$ = 0.173 ± 0.006; number of examined dendrites: 36 p140Cap$^{+/+}$, 43 p140Cap$^{-/-}$; 3 independent experiments, data are presented as mean ± SEM. Unpaired *t*-test, p = 0.0003), indicating that not only the release properties at inhibitory terminals but also the ability to form inhibitory synapses on target neurons is changed in neurons lacking p140Cap.

p140Cap$^{-/-}$ Cultures Display Abnormal Spontaneous Firing Properties and Enhanced Network Synchronization During Neuronal Maturation

To investigate whether the increased number of functional inhibitory synapses affects network activity during neuronal maturation in p140Cap$^{-/-}$ neurons, we compared the electrical properties of p140Cap$^{+/+}$ and p140Cap$^{-/-}$ hippocampal networks using micro-electrode arrays (MEAs). Spontaneous firing of hippocampal neurons was monitored at 2 developmental stages (9 and 18 DIV) in order to assess the maturation of the network. As shown previously (Gavello et al. 2012), the firing properties of hippocampal neurons vary significantly with time in these conditions. Spontaneous activity is mainly characterized by an asynchronous spike train activity with limited number of bursts in immature cultures, that switches to a burst activity characterized by a higher degree of synchronization in mature cultures.

The firing frequency at 9 DIV was significantly lower in p140Cap$^{-/-}$ (0.50 ± 0.05 Hz, n = 11 MEA, 277 channels, 3 independent experiments) with respect to controls (0.74 ± 0.11 Hz, n = 5 MEA; 400 channels, 3 independent experiments, P = 0.022 unpaired *t*-test) (Fig. 3*A*,*B*). On the contrary, at 18 DIV the absence of p140Cap induced a 3-fold increase in firing frequency compared to controls (2.55 ± 0.13 Hz vs. 0.87 ± 0.05 Hz, respectively; P < 0.0001, unpaired *t*-test) (Fig. 3*C*,*D*). In addition, the number of bursts (12.3 ± 0.5 vs. 6.2 ± 0.4, P < 0.0001, unpaired *t*-test) and the burst duration (0.36 ± 0.04 vs. 0.09 ± 0.004 s, P < 0.0001, unpaired *t*-test) were significantly larger in p140Cap$^{-/-}$ neurons with respect to controls (Fig. 3*E*,*F*).

Besides monitoring simultaneously the activity of many neurons (60 or more), MEA recordings allow to evaluate the degree of synchronization of neuronal networks during culture maturation (Gavello et al. 2012). We found that p140Cap$^{-/-}$ neurons exhibited synchronized activity at earlier stages than the control. p140Cap$^{-/-}$ neurons displayed an increased synchronism at 9 DIV that was absent in control neurons of the same age. This effect was clearly visible when comparing the raster plots, where action potentials (AP) monitored by each active recording channel are converted in a sequence of vertical lines versus time, and by the relative cross-correlation peak. In 9 DIV control neurons, AP activity is distributed randomly over time (Fig. 3*G*, left plot), becoming more synchronized at 18 DIV, when nearly all recording channels display synchronous AP bursts for tens of seconds (Fig. 3*I*, left plot). Conversely, p140Cap$^{-/-}$ neurons displayed, already at 9 DIV, robust synchronous firing (Fig. 3*G*, right plot), that increased at 18 DIV

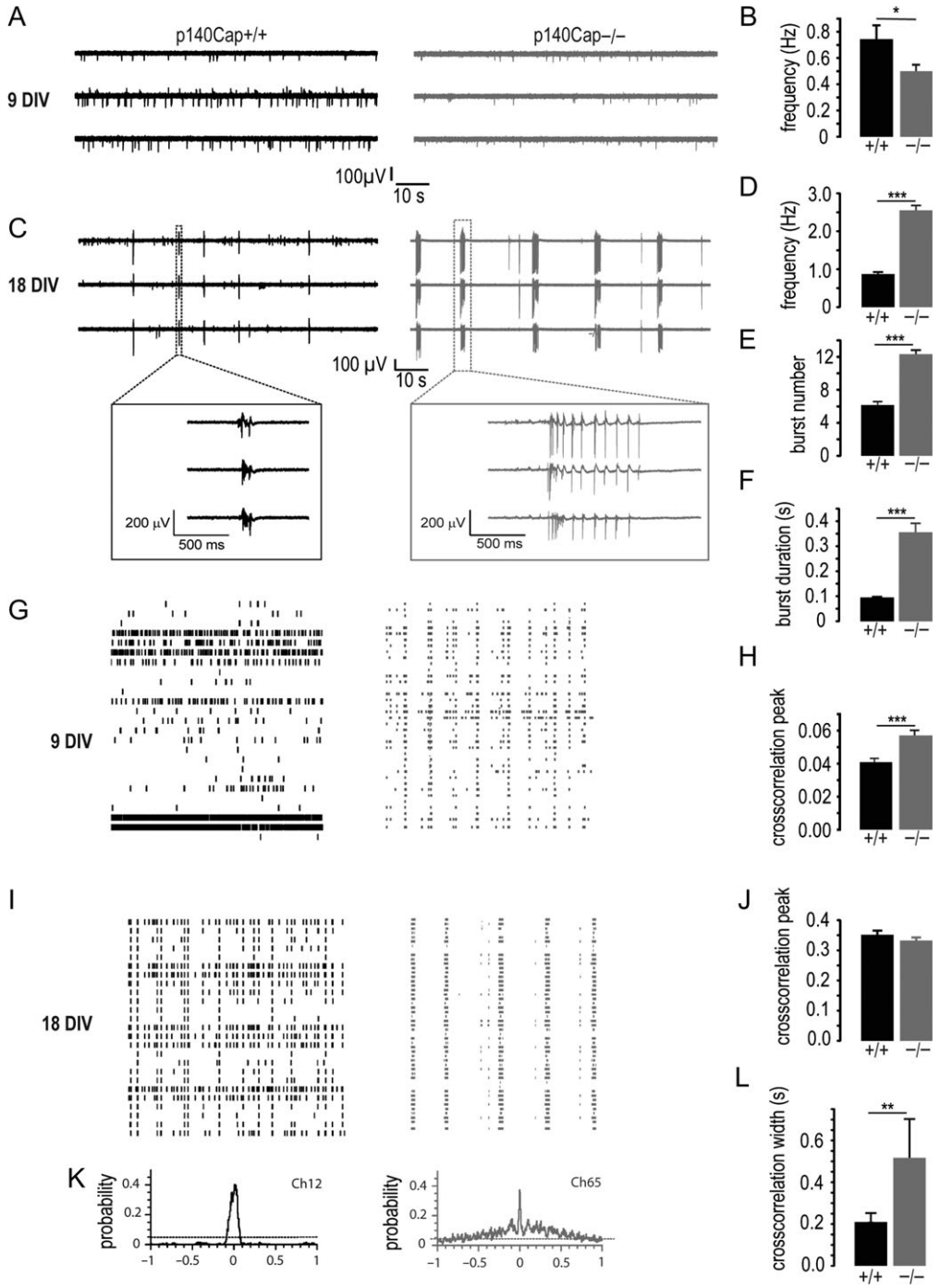

Figure 3. MEAs analysis on 9 and 18 DIV hippocampal neurons from p140Cap$^{+/+}$ and p140Cap$^{-/-}$ mice. (*A*) Representative traces of spontaneous firing from primary hippocampal neurons at 9 DIV measured with conventional micro-electrode arrays (MEAs). p140Cap$^{+/+}$ traces are shown in black (left) while p140Cap$^{-/-}$ traces are in gray (right). (*B*) Firing frequency (phasic) was significantly smaller in p140Cap$^{-/-}$ (as compared to control neurons at 9 DIV). (*C*) At 18 DIV spikes were principally grouped in bursts. This was the case for p140Cap$^{+/+}$ as well as for p140Cap$^{-/-}$ neurons. The insets at the bottom are a representation of the events indicated by the rectangle at an enlarged timescale. (*D*) Quantification of firing frequency at 18 DIV. (*E*, *F*) Burst number and burst duration. (*G*) Representative raster plots from MEA recordings of primary hippocampal networks at 9 DIV from p140Cap$^{+/+}$ (black traces) and p140Cap$^{-/-}$ neurons (gray traces). (*H*) Mean cross-correlation peaks at 9 DIV in p140Cap$^{-/-}$ neurons compared to controls. (*I*, *J*) Same as for panel (*G*) and (*H*) but for 18 DIV neurons. (*K*) Representative time course of the cross-correlation function recorded for p140Cap$^{+/+}$ from channel 12 and p140Cap$^{-/-}$ neurons from channel 65. (*L*) Mean width of the cross-correlation function obtained from p140Cap$^{+/+}$ and p140Cap$^{-/-}$ neuronal networks.

(Fig. 3*I*, right plot), as shown by the relative correlation peak (Fig. 3*H*). Firing activity was evident in a large number of recording channels (80 ± 5% vs. 81 ± 8%, respectively) and was highly synchronous in both p140Cap$^{+/+}$ and p140Cap$^{-/-}$ neuronal networks, suggesting that at 18 DIV comparable areas of both networks were effectively interconnected. The mean cross-correlation peak estimated from the recording channels were high in both cases (0.35 ± 0.2 vs. 0.32 ± 0.2, respectively)

(Fig. 3J), but exhibited a significantly different shape (Fig. 3K). In control neurons the cross-correlation function was significantly narrow (mean width at 0.05 was 197 ± 57 ms; $n = 7$ MEA), while in p140Cap$^{-/-}$ neurons the cross-correlation function after peaking at a maximal value at $t = 0$ persisted for longer times (mean width at 0.05 was 520 ± 185 ms, $n = 13$ MEA; $P = 0.0001$, unpaired t-test) (Fig. 3L). This time-extended strong correlation results most likely from the prolonged bursting activity of neurons in the absence of p140Cap, and ensures a more effective synchronous activity within the network.

p140Cap$^{-/-}$ Mice are more Susceptible to 4-Aminopyridine-induced Seizures In Vitro and to Kainate-induced Seizures In Vivo

The finding that knocking out p140Cap leads to higher hippocampal network synchronization at early times in cultured hippocampal neurons prompted us to test the ability of p140Cap$^{-/-}$ mice to develop seizure-like events (SLEs). We first induced SLEs in vitro using brain horizontal slices containing the hippocampus and the entorhinal cortex (EC), extracellularly perfused with the pro-convulsive compound 4-aminopyridine (4-AP). Local field potential (LFP) recordings (Fig. 4A and inset below) were performed by placing the tip of artificial cerebrospinal fluid (ACF)-filled glass pipettes in the CA1 area of the hippocampus and in layer II–III of the EC. A few minutes after starting the perfusion, tonic-clonic SLEs became detectable in 5 out of 14 p140Cap$^{+/+}$ slices (36%). Interestingly, a larger percentage of p140Cap$^{-/-}$ slices (6 out of 8, 75%) displayed 4-AP-induced SLEs as compared to p140Cap$^{+/+}$ preparations ($p = 0.031$, z-test for 2 population proportions) (Fig. 4B). Furthermore, the average number of SLEs per minute was significantly higher in p140Cap$^{-/-}$ than in control slices (0.34 ± 0.04 vs. 0.19 ± 0.03, respectively, $N = 6$ slices from 3 p140Cap$^{-/-}$ mice and $N = 5$ slices from 3 p140Cap$^{+/+}$ mice, $p = 0.038$, unpaired t-test) (Fig. 4C). Conversely, the average SLE duration was not different in the 2 groups (p140Cap$^{+/+}$: 31 ± 10 s, p140Cap$^{-/-}$: 39 ± 6 s, unpaired t-test, $p = 0.9$) (Fig. 4D). These results demonstrate that a higher hippocampal network synchronization is sufficient to make p140Cap$^{-/-}$ hippocampal slices perfused with 4-AP more prone to develop seizure-like events.

We then analyzed if seizure susceptibility is altered in p140Cap$^{-/-}$ mice in vivo after kainic acid (KA) treatment. Figure 4E shows the time course of the behavioral response of p140Cap$^{+/+}$ and p140Cap$^{-/-}$ mice to 35 mg/kg KA over a 3-h period after i.p. administration. In all mice, this dose of KA resulted in immobility and staring within the first 10 min, followed by head bobbing and stereotyped movements (stage 2 and 3 of Racine's scale) (Bozzi et al. 2000). 20 min after KA injection, p140Cap$^{-/-}$ mice rapidly progressed to stage 5 and 6 and showed continued generalized activity, while only 50% p140Cap$^{+/+}$ mice slowly reached stage 5 (genotype as between-subject factor and time within subject factor; effect of time: $F = 9{,}67$, $p = 0.0001$; effect of genotype: $F = 12.29$, $p = 0.0057$, 2-way repeated measure analysis of variance followed by Bonferroni post hoc test). Overall, the latency to the first stage 5 (status epilepticus) seizure differed between p140Cap$^{+/+}$ (70.3 ± 0.3 min, $N = 3$) and p140Cap$^{-/-}$ mice (26.6 ± 3.3 min, $N = 3$; $p = 0.0002$, unpaired t-test) (Fig. 4F). Mortality rate following KA administration was strongly different between control and p140Cap$^{-/-}$ mice (p140Cap$^{+/+}$ 0/7; p140Cap$^{-/-}$ 5/7 stats). Thus, the progression of clinical signs following KA treatment was dramatically different in control and knockout animals.

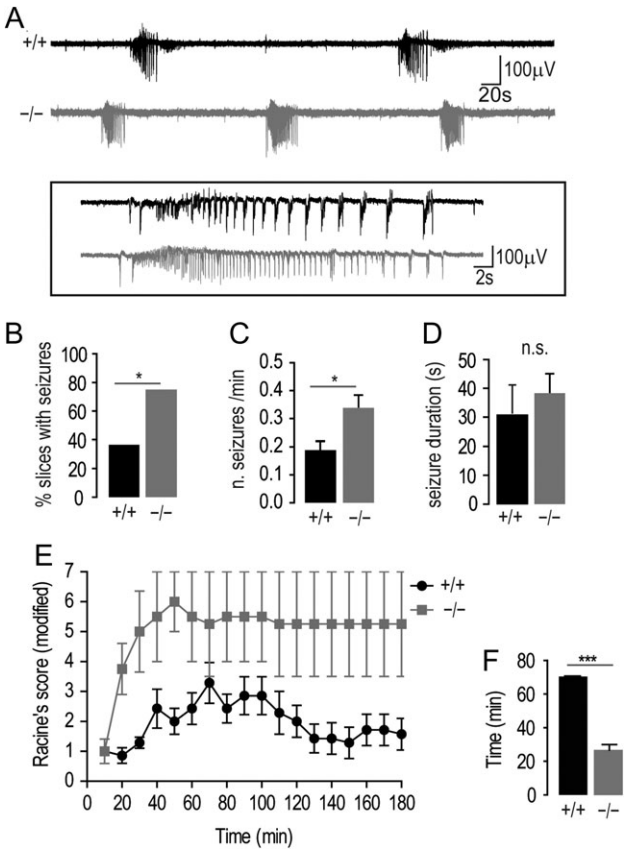

Figure 4. Seizure susceptibility in p140Cap$^{+/+}$ and p140Cap$^{-/-}$ mice. (*A*) Representative LFP traces recorded in the hippocampus of p140Cap$^{+/+}$ (black) and p140Cap$^{-/-}$ (gray) mice during bath perfusion with 4-AP (100 mM). The inset below shows enlarged individual ictal discharges. (*B*) Summary of the total percentage of slices showing detectable seizure-like activity (SLE). (*C*) Average SLE frequency. (*D*) Average SLE duration in p140Cap$^{+/+}$ and p140Cap$^{-/-}$. (*E*) Progression of behavioral changes after systemic KA administration (35 mg/kg, i.p.) in p140Cap$^{+/+}$ and p140Cap$^{-/-}$ mice over a 3 h observation period. Data represent mean seizure scores ± SEM. (*F*) Latency to the first Stage 5: comparison between p140Cap$^{+/+}$ and p140Cap$^{-/-}$ shows that mutant animals need less time to reach status epilepticus.

p140Cap$^{-/-}$ Mice Display Higher Density of Inhibitory Synapses in the Hippocampus

To verify whether the enhanced inhibitory synapse density described in p140Cap$^{-/-}$ cultures (Fig. 2E) was also present in the intact brain, we measured the density of inhibitory VGAT-positive synapses in the CA1 region of both control and p140Cap$^{-/-}$ hippocampi by immunofluorescence and confocal microscopy (Fig. 5A, a-c). We found a significant increase of both the density and size of VGAT puncta in CA1 of mutant mice compared to controls (Number of VGAT puncta/μm2: p140Cap$^{+/+}$ = 0.059 ± 0.004, p140Cap$^{-/-}$ = 0.080 ± 0.005; area of VGAT puncta on field area: p140Cap$^{+/+}$ = 0.016 ± 0.002, p140Cap$^{-/-}$ = 0.034 ± 0.004, $n = 5$ p140Cap$^{+/+}$ mice, $n = 5$ p140Cap$^{-/-}$ mice; Mann–Whitney Rank Sum Test $p = 0.019$ for density; $p = 0.003$ for area analysis) (Fig. 5B,C). To confirm these data, we also performed an electron microscopic analysis of perisomatic synapses in the same hippocampal region (Fig. 5D). We found a significant increase of the number of symmetric synaptic appositions surrounding the cell body of CA1 pyramidal neurons in p140Cap$^{-/-}$ versus age-matched control mice (number of perisomatic symmetric synapse per 100 μm:

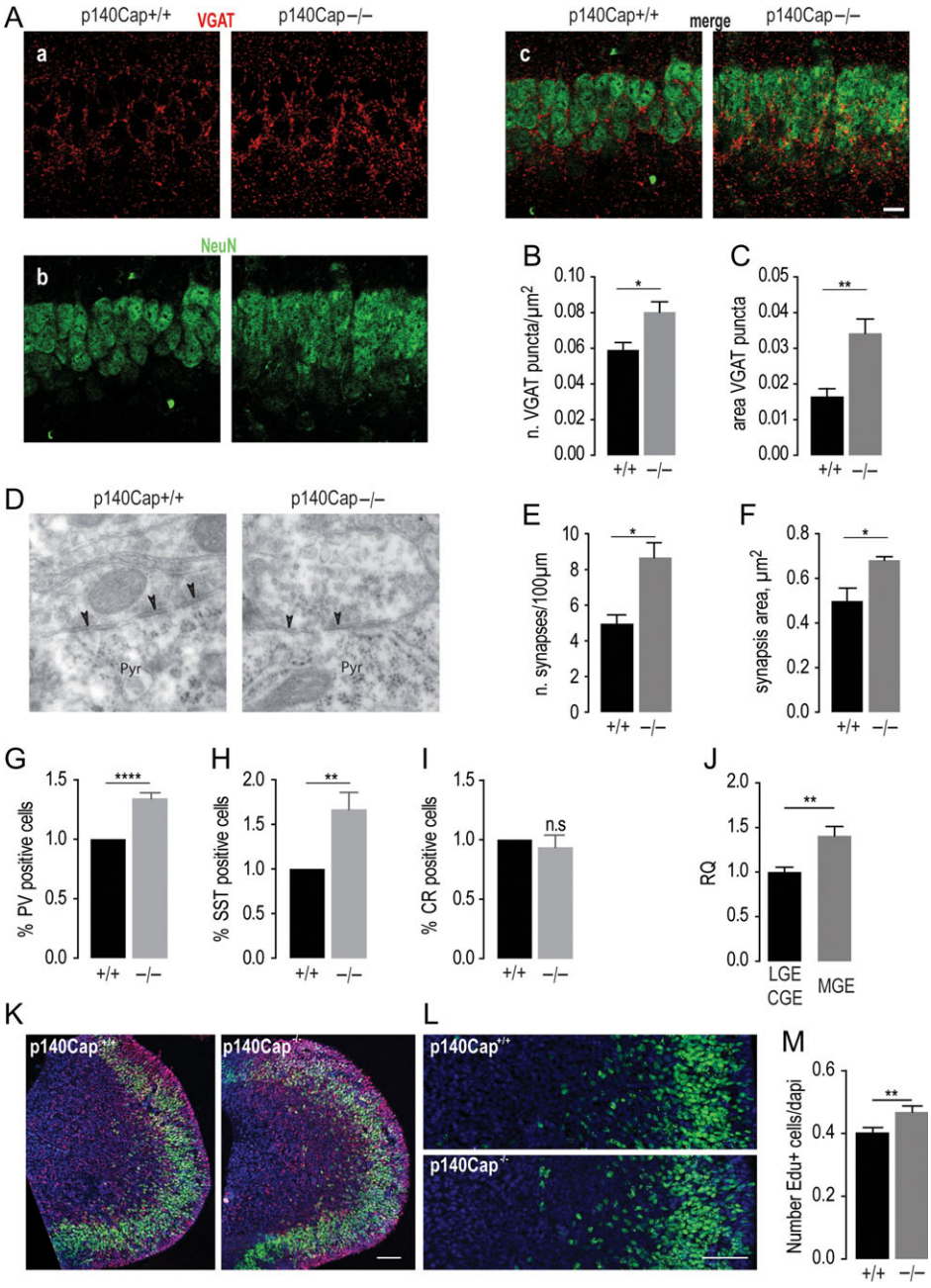

Figure 5. Quantification of VGAT inhibitory synapses and EdU analysis in p140Cap$^{+/+}$ and p140Cap$^{-/-}$ mice. (A) Representative immunofluorescence pictures of VGAT puncta in the CA1 region of 2-month-old p140Cap$^{+/+}$ and p140Cap$^{-/-}$ hippocampi (panel a). NeuN was used as marker (panel b). Merge is shown in panel c. Scale bar = 10 µm. (B) and (C) Quantification of VGAT density (B) and total area of VGAT puncta/area field (C). (D) Representative electron microscopy pictures of hippocampal CA1 region of perisomatic inhibitory synapses in 2-month-old mice. Arrows indicates symmetric synaptic appositions. (*E*) and (*F*) Quantification of density (*E*) and area (*F*) Scale bar. (*G*)–(*I*). Percentage quantification of Parvalbumin (PV) (*G*), Somatostatin (SST) (*H*) and Calretinin (CR) (*I*) positive cells in the CA1 region of the 2 genotypes. (*J*) Quantitative real-time RT-PCR analysis of p140Cap transcript in E15.5 CGE + LGE and MGE from p140Cap$^{+/+}$ embryos. (*K*) Representative immunofluorescence pictures of E12.5 total MGE stained for EdU (green nuclei), Nkx2.1 (red nuclei) and DAPI (blue nuclei) from p140Cap$^{+/+}$ and p140Cap$^{-/-}$ mice. Scale bar = 50 µm. (*L*) Cropped-Horizontal section of MGE from p140Cap$^{+/+}$ and p140Cap$^{-/-}$, with green cells representing EdU-positive cells and DAPI staining for nuclei. Scale bar = 50 µm. (*M*) Quantification of EdU-positive cells on DAPI-positive cells from panels L.

p140Cap$^{+/+}$ 5 ± 0.6, $N = 3$; p140Cap$^{-/-}$ 8 ± 0.76 $N = 3$; $p = 0.019$) (Fig. 5*E*). Moreover, the size of GABAergic terminals establishing perisomatic synapses was also increased in mouse mutants (p140Cap$^{+/+}$ 0.498 ± 0.059 µm^2 $N = 3$; p140Cap$^{-/-}$ 0.682 ± 0.016 µm^2 $N = 3$; $p = 0.039$) (Fig. 5*F*). These results indicate that both p140Cap-depleted neuronal cultures and p140Cap$^{-/-}$ mice display an increased number of inhibitory synapses impinging on CA1 pyramidal neurons.

To further characterize the inhibitory interneuron network in the hippocampus, we quantified 3 major classes of INs, i.e., Parvalbumin (PV), Somatostatin (SST) and Calretinin (CR) positive cells. This analysis was performed in the CA1 region of 8-week-old p140Cap$^{+/+}$ and p140Cap$^{-/-}$ mice using specific antibodies (see Supplemental Fig. 1 for representative images of the 2 genotypes). We observed a significant increase in the number of PV+ cells (≥34,1%, unpaired *t*-test $p < 0.0001$) (Fig. 5*G*), and

SST+ cells (≥66,4%, unpaired *t*-test $p = 0.0065$) (Fig. 5*H*) in p140Cap$^{-/-}$ mice with respect to p140Cap$^{+/+}$ mice, whereas the number of CR+ interneurons was unchanged (≤6,6% unpaired *t*-test $p = 0.543$ n.s.) ($n = 5$ p140Cap$^{+/+}$ mice, $n = 5$ p140Cap$^{-/-}$ mice) (Fig. 5*I*).

p140Cap$^{-/-}$ Mice Display Increased Number of Actively cycling Interneuron Progenitors in MGE

Hippocampal GABAergic interneurons originate from the ganglionic eminences (GE), which are transitory embryonic structures in the developing ventral telencephalon (Tricoire et al. 2011). It is known that interneuron diversity largely emerges from spatially segregated progenitor cells with distinct transcriptional profiles in the medial, caudal and lateral ganglionic eminence (MGE, CGE and LGE). Respectively, the MGE gives rise to the large majority of PV- and SST-expressing interneurons, while CR+ cells mostly originate from CGE (Gelman and Marín 2010; Maroof et al. 2010; Vaghi et al. 2014). For these reasons, we analyzed the expression profile of p140Cap transcript in both MGE and CGE + LGE in E15.5 p140Cap$^{+/+}$ embryos using qRT-PCR. Results indicated that the p140Cap mRNA is significantly enriched in MGE region compared to CGE + LGE (Fig. 5*J*). The MGE versus the CGE + LGE were further identified by the expression of the specific markers Nkx2.1 and Coup II, respectively (Supplemental Fig. 2*A*). Moreover, immunofluorescence and confocal analysis confirmed the presence of the p140Cap protein in the MGE already at E12.5 stage (Supplemental Fig. 2*B*), with a major intensity gradient in the Sub-Ventricular zone (SVZ), compared to the Ventricular zone (VZ). These observations suggest that p140Cap may play a specific role in the niche were PV+ and SST+ cells originate during development

To verify whether deletion of p140Cap affects the dynamic equilibrium between cell proliferation and cell death in Nkx2.1 progenitors, we quantified the number of actively cycling interneuron progenitors on MGE sections of E12.5 embryonic brains. This experiment revealed a small, but statistically significant increase (about 15%) in the number of BrdU-positive cells in the ventricular zone of p140Cap$^{-/-}$ mice compared to controls (p140Cap$^{+/+}$ 0.403 ± 0.016 $n = 7$; p140Cap$^{-/-}$ 0.469 ± 0.018 $n = 4$; unpaired *t*-test $p = 0.009$) (Fig. 5*K*–*M*). Analysis of TUNEL-positive cells in MGE at the same time point did not disclose any significant difference between the 2 genotypes, indicating that the processes of cell survival and apoptosis are not affected by the lack of p140Cap (Supplementary Fig. 2*C*). Indeed we found a very small percentage of TUNEL-positive cells at this stage (less than 0.1% of total number of cells), suggesting that apoptosis is not a primary event at this developmental stage. Interestingly, in p140Cap$^{-/-}$ MGE, a higher number of Nkx2.1-positive nuclei, the specific marker of MGE-interneuron progenitors, has been detected not only in the ventricular zone (VZ) but also in the sub-ventricular zone (SVZ) and in the mantle zone (MZ), 2 areas where in normal conditions, the process of cell-cycle exit and differentiation should be already started (Supplementary Fig. 2*D*, *E*).

Specific Ablation of p140Cap in Forebrain INs Leads to Higher Susceptibility to Develop Seizures In Vitro and Increased Density of Inhibitory Synapses

To investigate the relevance of p140Cap in the inhibitory network, we generated a conditional mouse model (hereafter called C-p140Cap) in which p140Cap is removed only in Dlx5/6-expressing INs by crossing p140Cap lox/lox mice with the Dlx5/6-Cre line (Supplementary Figure 3*A*,*B*). Confocal analyses of C-p140Cap mice revealed a 42% increase in the density of VGAT puncta in the CA1 region of the hippocampus (VGAT puncta per μm^2, Flox-p140Cap: 0.166 ± 0.017 $n = 5$, C-p140Cap: 0.245 ± 0.024 $n = 4$; unpaired *t*-test $p = 0.0293$) as well as an increase in the size of VGAT-positive structures (VGAT puncta area on field area-normalized value, Flox-p140Cap: 0.089 ± 0.001, C-p140Cap 0.10 ± 0.003; $n = 5$ mice per genotype; unpaired *t*-test $p = 0.0017$) (Fig. 6*A*,*B*). C-p140Cap mice also displayed higher susceptibility to 4-aminopyridine-induced seizures in vitro, as assessed by the increased frequency of ictal events (Flox-p140Cap frequency: 0.23 ± 0.05 SLE/minute, $n = 11$ slices in 4 mice, C-p140Cap: 0.34 ± 0.04 SLE/minute, $n = 10$ slices in 4 mice, p 0.034, unpaired *t*-test; Flox-p140Cap SLE duration: 69 ± 11 s, $n = 11$ slices in 4 mice, C-p140Cap: 75 ± 12 s, $n = 10$ slices in 4 mice, $p = 0.728$, unpaired *t*-test) (Fig. 6*C*,*D*). However, seizures susceptibility after kainic acid treatment in vivo (Supplementary Fig. 4*A*), number of PV+ and SST+ interneurons in the hippocampus (Supplementary Fig. 4*B*) and number of proliferating interneuron progenitors in MGE of E12.5 embryos (Supplementary Fig. 4*C*) are not altered in C-p140Cap mice with respect to control Flox-p140Cap mice. These data indicate that selective removal of p140Cap from inhibitory interneurons, by using Dlx5/6-Cre line, enhances inhibitory synaptogenesis and alters E/I balance in hippocampal circuits without affecting some of the early events occurring in the IN progenitors pool, such as the number of proliferating Nkx2.1-positive cells.

Discussion

In the present study, we demonstrate that the adapter protein p140Cap plays a fundamental role in the development and refinement of the inhibitory network by regulating both the number and the activity of GABAergic synapses.

We and others have previously demonstrated that p140Cap is involved in the organization of the excitatory postsynaptic density (Sheng and Hoogenraad 2007; Tomasoni et al. 2013; Repetto et al. 2014; Fossati et al. 2015; Alfieri et al. 2017) and eventually plays a central role in learning and memory processes (Jaworski et al. 2009; Repetto et al. 2014). Indeed p140Cap$^{-/-}$ mice display impaired LTP and defective establishment and consolidation of new declarative memories (Repetto et al. 2014). At the cellular and molecular level the lack of p140Cap leads to the disruption of dendritic spine integrity (Jaworski et al. 2009; Tomasoni et al. 2013) which may be responsible for the LTP defect in hippocampal slices (Repetto et al. 2014). These studies pointed to a role for this protein in the molecular organization of excitatory synapses and indicated that p140Cap acts as a hub for postsynaptic complexes relevant to psychiatric and neurological disorders (Alfieri et al. 2017).

We here report that p140Cap is present in GABAergic presynaptic structures and its ablation results in altered GABAergic inhibitory neurotransmission (increased mIPSC frequency and GABA release) and increased number of inhibitory synapses impinging on pyramidal neurons. Therefore p140Cap regulates the developmental assembly of inhibitory circuits. Of note, some of the proteins localized in the inhibitory compartment were identified in the p140Cap synaptic interactome (Alfieri et al. 2017).

Interneurons are local circuit cells mainly responsible for inhibitory activity in the adult hippocampus, thereby controlling the activity of the principal excitatory cells (Trygve et al. 2007) and regulating the proper E/I balance (Freund and Buzsáki

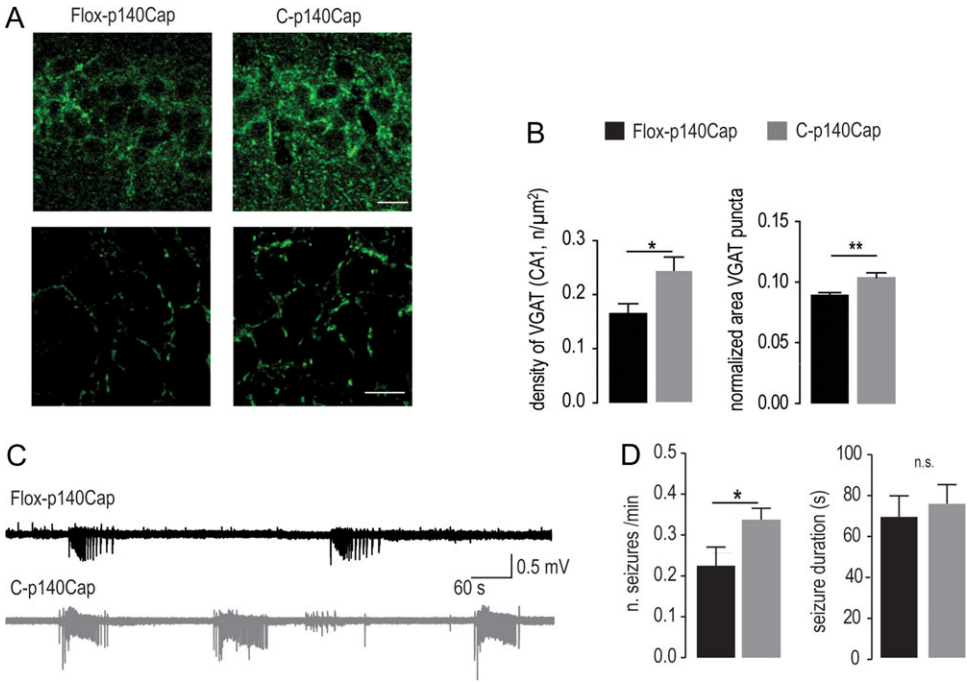

Figure 6. Selective removal of p140Cap from inhibitory interneurons affects the inhibitory compartment. (*A*) Representative VGAT immunofluorescence in CA1 hippocampal region of control (Flox-p140Cap) (left panels) and p140Cap conditional (C-p140Cap) (right panels) brain slices. Lower panels are a high magnification of the inset. Scale bar value = 10 μm. (*B*) VGAT-positive puncta density in Dlx5/6-Cre slices compared to controls and total area of VGAT puncta/area field. (*C*) Representative LFP traces recorded in the hippocampus of Flox-p140Cap and C-p140Cap mice during bath perfusion with 4-AP (100 μM). Calibration: 500 μV, 60 s. (*D*) The average SLE frequency, but not duration, was found significantly increased in p140Cap conditional brain slices compared to their controls.

1996; Somogyi and Klausberger 2005). In addition, they strongly regulate neocortical development by modulating several cellular processes such as neuronal proliferation, migration, differentiation and connectivity. Notably, altered inhibition results in pathological rearrangements which are responsible, in general, for impaired neuronal development (Tyzio et al. 2006, 2014; Gogolla et al. 2009), altered circuitry formation (Antonucci et al. 2012; Berryer et al. 2016) and abnormal neuronal plasticity (Hensch 2005; Harauzov et al. 2010; Succol et al. 2012; Deidda et al. 2015). In agreement, several developmental brain disorders such as autism, intellectual disability and schizophrenia result from an imbalanced E/I tone and are associated with alterations in GABAergic neurotransmission (Hashimoto et al. 2005; Tabuchi et al. 2007; Coghlan et al. 2012).

Several recent studies have demonstrated that fast synaptic inhibition mediated by different types of GABA releasing interneurons is also important for the generation of network oscillations, i.e., the neuronal activity generating network synchrony. This optimal brain status is essential to strengthen information processing and cognitive functions and to prevent a wide range of neurological diseases including epilepsy, schizophrenia, and autism spectrum disorders (ASDs) (for review see Coghlan et al. 2012; Marín 2012; Rapanelli et al. 2017). Synchronicity is one of the requisites of a functional neuronal network and GABAergic interneurons are the key players of this phenomenon through multiple mechanisms, including the depolarizing action of GABA during brain development, transient synaptic connections, extrasynaptic transmission, gap junction coupling, and the presence of pacemaker-like neurons (Blankenship et al. 2009; Bonifazi et al. 2009). Dysfunctions concerning some of those molecular mechanisms could be at the basis of the aberrant phenotype that we observe in p140Cap$^{-/-}$ models such as the cognitive and memory defects (Repetto et al. 2014).

Our results indicate that the absence of p140Cap results in a significant increase in neuronal network firing and synchronization, which are crucial for neuronal information processing and storage in the hippocampus (Chen et al. 2005; Li et al. 2007). Of note, spontaneous synchronized bursts were detected in p140Cap$^{-/-}$ neuronal networks both in vivo and in vitro. Indeed, differently from p140Cap$^{+/+}$ neuronal networks, which produce spontaneous synchronized bursts mostly after 2 weeks of cell seeding, p140Cap$^{-/-}$ cells exhibited synchronized activity already at 9 DIV, a time window where control neurons fire mostly in single-spike fashion. In line with the higher hippocampal network synchronization, both the global deletion of p140Cap or the selective removal of the protein from forebrain interneurons resulted in increased susceptibility to pharmacological-induced protocols of epilepsy.

Besides resulting in increased ability to form inhibitory synapses, the genetic ablation of p140Cap during brain development results in increased number of inhibitory interneurons—in particular the PV$^+$ and SST$^+$ cells—in CA1 hippocampal region, suggesting that the process of interneuron generation during development may be controlled by this protein. Of note, both p140Cap transcript and protein are already present at E12.5 in the MGE, the embryonic region where PV$^+$ and SST$^+$ interneurons originate (see also Supplementary Fig. 2A), thus opening the possibility that p140Cap may regulate neural progenitor proliferation as well as the process of interneuron migration out of MGE. The adapter protein p140Cap has been recently demonstrated to interfere with growth factor-dependent signaling in breast cancer cells, by inhibiting proliferative signals, such as the EGF-dependent Ras/Erk1/2 signaling (Damiano et al. 2010). In particular, in transformed cells, p140Cap expression limits tumor growth and confers the ability to activate the apoptotic program restoring mammary gland

tissue morphogenesis (Mailleux et al. 2007; Grasso et al. 2017). Therefore, in neuron precursors, p140Cap deficiency might affect the dynamic equilibrium between cell proliferation and cell differentiation in Nkx2.1 progenitor cells. The higher number of EdU-positive cells, which is not accompanied by a decreased cellular apoptosis, in the ventricular zone of p140Cap$^{-/-}$ mice may thus account for the increased number in MGE-derived parvalbumin and somatostatin interneurons in the hippocampus of p140Cap$^{-/-}$ mice. This is also consistent with the presence of Nkx2.1-positive nuclei of MGE-interneuron progenitors in the p140Cap$^{-/-}$ SVZ, where in normal conditions, the process of cell-cycle exit and differentiation should be already started (see Supplementary Fig. 2*D*,*E*). As an alternative mechanism, p140Cap has been recently found to stabilize E-cadherin at the cell membrane (Damiano et al. 2010). On neurons, the same E-cadherin is crucial for interneuron differentiation and correct guidance towards the cortex. Finally, the p140Cap-dependent inhibition of EGFR and Erk1/2 signaling observed in tumor cells (Damiano et al. 2010) may also account for the aberrant inhibitory synaptogenesis in GABAergic interneurons in p140Cap KO hippocampi. In recent times, different factors have been implicated in the control of inhibitory synaptogenesis, including Neuregulin 2 (Lee et al. 2015), FGF7 (Dabrowski et al. 2015), Semaphorin 4D (Kuzirian et al. 2013), SYNGAP1 (Berryer et al. 2016), and most notably BDNF (Bath et al. 2012). Of note, all these factors may require, for their action, KRAS-ERK1/2 mediated signaling and indeed an up-regulation of ERK signaling during early phases of postnatal development leads to a selective enhancement of synaptogenesis in GABAergic interneurons (Papale et al. 2017).

As already mentioned, interneuron defects are known to represent one of the main causes of brain development disorders and are also involved in neurodegenerative or injury-based disorders (Hunt and Baraban 2015). In epilepsy, the synchronization of neuronal firing involves the interaction of GABAergic inhibitory and glutamatergic excitatory mechanisms (Wu et al. 2015). In this pathological situation, fundamental disturbance in the E/I balance may result in abnormal activity of forebrain-neuronal circuits, which over time leads to epileptogenesis. Even if the role of interneurons in epilepsy is still discussed, the results of recent studies have stressed the importance of GABAergic neurons in triggering this phenomenon (Yekhlef et al. 2015; Avoli et al. 2016). In fact, activation of PV$^+$ interneurons appears to generate sustained epileptic events (Shiri et al. 2015; Yekhlef et al. 2015) and contribute to their maintainance (Ellender et al. 2014); (Khoshkhoo et al. 2017). Since these cells largely mediate synaptic inhibition, their proepileptic effect may sound counterintuitive. However, synchronous activation of groups of PV$^+$ and SST$^+$ interneurons results in a transient increase in extracellular potassium concentration ([K+]^o), which mediates membrane potential depolarization (Yekhlef et al. 2015). Such depolarization at times reaches a critical threshold for action potential firing in a relatively large number of surrounding cells (including principal glutamatergic neurons), inducing a massive activation and a further increase in [K+]^o. This phenomenon marks the initial stage of a seizure, which continues as the network keeps firing in a synchronous fashion and possibly propagates by recruiting further neighboring areas. In addition to their ability to start seizures using a non-synaptic effect (i.e., the [K+]^o increase), GABAergic interneurons may contribute to seizure maintenance as their continuous release of GABA eventually leads to an increase in chloride concentration in postsynaptic cells, resulting in a depolarizing shift in Cl^- reversal potential and consequently in an excitatory, rather than inhibitory, effect of GABA (Huberfeld et al. 2007; Kaila et al. 2014). These evidences are in line with the increased susceptibility of p140Cap$^{-/-}$ mice to epileptogenic agents, even though their hippocampal network is enriched in the inhibitory component.

Notably selective removal of p140Cap in the Dlx5/6-expressing interneurons does not affect the number of interneuron progenitors in MGE and of mature PV$^+$ and SST$^+$ interneurons in the hippocampus, as well the susceptibility to kainic acid-induced seizures in vivo, suggesting that either p140Cap may contribute to some molecular events occurring in the progenitor pool before Dlx5/6-driven Cre expression, in particular the mitotic competence of the progenitors, or that the presence of p140Cap in populations other than INs is relevant for a correct INs function. The use of additional models (Taniguchi et al. 2011) may help to elucidate the role of p140Cap expression in early phases of INs development.

This work puts therefore the basis to further investigating the role of p140Cap in defining the E/I balance during hippocampal circuitry definition and the synaptopathies associated with its absence.

Supplementary Material

Supplementary data is available at *Cerebral Cortex* online.

Funding

This work was supported by MIUR (Ministero Università Ricerca, PRIN (Progetti Interesse Nazionale) grant 20108MXN2J_004, 2015XS92CC to P.D.), AIRC (Associazione Italiana Ricerca Cancro) to P.D. (IG-15399); Compagnia San Paolo, Torino; Progetto d'Ateneo, Università di Torino 2011 to P.D. and E.T.; MIUR (PRIN grant 2010JFYFY2 to E.C. and grant 2015FNWP34_005 to V.C.), SanPaolo Foundation (grant CSTO165284 to V.C.) and Telethon Foundation (grant # GGP15110 to E.C.). Cariplo (2012-0560 and 2015-0594 to M.M.), Regione Lombardia-CNR 2017-2019 and Italian Ministry of Health GR-2011-02347377 to M.M.; Progetto Bandiera Interomics 2015-2017 to E.M.; Fondazione Vodafone 2017-2018 to E.M and M.M; I.C. was supported by Fondazione Giancarla Vollaro, E.F. by Fondazione Cariplo 2012-0560.Telethon Foundation (grant GGP15098 to M.G.), AIRETT (Associazione Italiana RETT), Associazione Albero di Greta ONLUS and International Foundation for CDKL5 Research to M.G.; Fondazione Telethon (GGP16234 to S.T.).

Notes

We thank the Monzino Foundation (Milano, Italy) for its generous gift of the LSM 510 Meta confocal microscope. This project has been approved by the Internal Bioethical Committee of the Department. *Conflict of Interest*: None declared.

References

Alfieri A, Sorokina O, Adrait A, Angelini C, Russo I, Morellato A, Matteoli M, Menna E, Boeri Erba E, McLean C, et al. 2017. Synaptic interactome mining reveals p140Cap as a new hub for PSD proteins involved in psychiatric and neurological disorders. Front Mol Neurosci. 10:212.

Allio A, Calorio C, Franchino C, Gavello D, Carbone E. 2015. Bud extracts from Tilia tomentosa Moench inhibit hippocampal neu- ronal fi ring through GABA A and benzodiazepine receptors activation. J Ethnopharmacol. 172:288–296.

Antonucci F, Turola E, Caleo M, Gabrielli M, Perrotta C, Novellino L, Clementi E, Giussani P, Viani P, Matteoli M, et al. 2012. Microvesicles released from microglia stimulate synaptic activity via enhanced sphingolipid metabolism. EMBO J. 31:1231–1240.

Avoli M, de Curtis M, Gnatkovsky V, Gotman J, Kohling R, Levesque M, Manseau F, Shiri Z, Williams S. 2016. Specific imbalance of excitatory/inhibitory signaling establishes seizure onset pattern in temporal lobe epilepsy. J Neurophysiol. 115:3229–3237.

Baldelli P, Hernandez-Guijo JM, Carabelli V, Carbone E. 2005. Brain-derived neurotrophic factor enhances GABA release probability and nonuniform distribution of N- and P/Q-type channels on release sites of hippocampal inhibitory synapses. J Neurosci. 25:3358–3368.

Baldelli P, Novara M, Carabelli V, Hernandez-Guijo JM, Carbone E. 2002. BDNF up-regulates evoked GABAergic transmission in developing hippocampus by potentiating presynaptic N- and P/Q-type Ca2+ channels signalling. Eur J Neurosci. 16:2297–2310.

Bath KG, Akins MR, Lee FS. 2012. BDNF control of adult SVZ neurogenesis. Dev Psychobiol. 54:578–589.

Berryer MH, Chattopadhyaya B, Xing P, Riebe I, Bosoi C, Sanon N, Antoine-Bertrand J, Levesque M, Avoli M, Hamdan FF, et al. 2016. Decrease of SYNGAP1 in GABAergic cells impairs inhibitory synapse connectivity, synaptic inhibition and cognitive function. Nat Commun. 7:13340.

Blankenship AG, Blankenship AG, Feller MB, Feller MB. 2009. Mechanisms underlying spontaneous patterned activity in developing neural circuits. Nat Rev Neurosci. 11:18–29.

Bonifazi P, Goldin M, Picardo MA, Jorquera I, Cattani A, Bianconi G, Represa A, Ben-Ari Y, Cossart R. 2009. GABAergic hub neurons orchestrate synchrony in developing hippocampal networks. Science. 326:1419–1424.

Bozzi Y, Vallone D, Borrelli E. 2000. Neuroprotective role of dopamine against hippocampal cell death. J Neurosci. 20:8643–8649.

Chen S, Yue C, Yaari Y. 2005. A transitional period of Ca2+-dependent spike afterdepolarization and bursting in developing rat CA1 pyramidal cells. J Physiol. 567:79–93.

Chin LS, Nugent RD, Raynor MC, Vavalle JP, Li L. 2000. SNIP, a novel SNAP-25-interacting protein implicated in regulated exocytosis. J Biol Chem. 275:1191–1200.

Coghlan S, Horder J, Inkster B, Mendez MA, Murphy DG, Nutt DJ. 2012. GABA system dysfunction in autism and related disorders: from synapse to symptoms. Neurosci Biobehav Rev. 36:2044–2055.

Corradini I, Donzelli A, Antonucci F, Welzl H, Loos M, Martucci R, De Astis S, Pattini L, Inverardi F, Wolfer D, et al. 2014. Epileptiform activity and cognitive deficits in SNAP-25(+/-) mice are normalized by antiepileptic drugs. Cereb Cortex. 24:364–376.

Dabrowski A, Terauchi A, Strong C, Umemori H. 2015. Distinct sets of FGF receptors sculpt excitatory and inhibitory synaptogenesis. Development. 142:1818–1830.

Damiano L, Di Stefano P, Camacho Leal MP, Barba M, Mainiero F, Cabodi S, Tordella L, Sapino A, Castellano I, Canel M, et al. 2010. p140Cap dual regulation of E-cadherin/EGFR cross-talk and Ras signalling in tumour cell scatter and proliferation. Oncogene. 29:3677–3690.

Deidda G, Parrini M, Naskar S, Bozarth IF, Contestabile A, Cancedda L. 2015. Reversing excitatory GABAAR signaling restores synaptic plasticity and memory in a mouse model of Down syndrome. Nat Med. 21:318–326.

Ellender TJ, Raimondo JV, Irkle A, Lamsa KP, Akerman CJ. 2014. Excitatory effects of parvalbumin-expressing interneurons maintain hippocampal epileptiform activity via synchronous afterdischarges. J Neurosci. 34:15208–15222.

Englot DJ, Modi B, Mishra AM, DeSalvo M, Hyder F, Blumenfeld H. 2009. Cortical deactivation induced by subcortical network dysfunction in limbic seizures. J Neurosci. 29:13006–13018.

Fossati G, Morini R, Corradini I, Antonucci F, Trepte P, Edry E, Sharma V, Papale A, Pozzi D, Defilippi P, et al. 2015. Reduced SNAP-25 increases PSD-95 mobility and impairs spine morphogenesis. Cell Death and Differ. 22:1425–1436.

Freund TF, Buzsáki G. 1996. Interneurons of the hippocampus. Hippocampus. 6:347–470.

Gavello D, Rojo-Ruiz J, Marcantoni A, Franchino C, Carbone E, Carabelli V. 2012. Leptin counteracts the hypoxia-induced inhibition of spontaneously firing hippocampal neurons: a microelectrode array study. PLoS One. 7:e41530.

Gelman DM, Marín O. 2010. Generation of interneuron diversity in the mouse cerebral cortex. Eur J Neurosci. 31:2136–2141.

Gogolla N, LeBlanc JJ, Quast KB, Südhof TC, Fagiolini M, Hensch TK. 2009. Common circuit defect of excitatory-inhibitory balance in mouse models of autism. J Neurodev Disord. 1:172–181.

Grasso S, Chapelle J, Salemme V, Aramu S, Russo I, Vitale N, Verdun L, Dallaglio K, Castellano I, Amici A, et al. 2017. The scaffold protein p140Cap limits ERBB2-mediated breast cancer progression interfering with Rac GTPase-controlled circuitries. Nat Commun. 8:1–16.

Harauzov A, Spolidoro M, DiCristo G, De Pasquale R, Cancedda L, Pizzorusso T, Viegi A, Berardi N, Maffei L. 2010. Reducing intracortical inhibition in the adult visual cortex promotes ocular dominance plasticity. J Neurosci. 30:361–371.

Hashimoto T, Bergen SE, Nguyen QL, Xu B, Monteggia LM, Pierri JN, Sun Z, Sampson AR, Lewis DA. 2005. Relationship of brain-derived neurotrophic factor and its receptor TrkB to altered inhibitory prefrontal circuitry in schizophrenia. J Neurosci. 25:372–383.

Hensch TK. 2005. Critical period plasticity in local cortical circuits. Nat Rev Neurosci. 6:877–888.

Huberfeld G, Wittner L, Clemenceau S, Baulac M, Kaila K, Miles R, Rivera C. 2007. Perturbed chloride homeostasis and GABAergic signaling in human temporal lobe epilepsy. J Neurosci. 27:9866–9873.

Hunt RF, Baraban SC. 2015. Interneuron transplantation as a treatment for epilepsy. Cold Spring Harbor Perspect Med. 5:a022376.

Ito H, Atsuzawa K, Sudo K, Di Stefano P, Iwamoto I, Morishita R, Takei S, Semba R, Defilippi P, Asano T, et al. 2008. Characterization of a multidomain adaptor protein, p140Cap, as part of a pre-synaptic complex. J Neurochem. 107:61–72.

Jaworski J, Kapitein LC, Gouveia SM, Dortland BR, Wulf PS, Grigoriev I, Camera P, Spangler SA, Di Stefano P, Demmers J, et al. 2009. Dynamic microtubules regulate dendritic spine morphology and synaptic plasticity. Neuron. 61:85–100.

Kaila K, Ruusuvuori E, Seja P, Voipio J, Puskarjov M. 2014. GABA actions and ionic plasticity in epilepsy. Curr Opin Neurobiol. 26:34–41.

Khoshkhoo S, Vogt D, Sohal VS. 2017. Dynamic, cell-type-specific roles for GABAergic interneurons in a mouse model of optogenetically inducible seizures. Neuron. 93:291–298.

Klausberger T, Somogyi P. 2008. Neuronal diversity and temporal dynamics: the unity of hippocampal circuit operations. Science. 321:53–57.

Kullmann DM. 2011. Interneuron networks in the hippocampus. Curr Opin Neurobiol. 21:709–716.

Kuzirian MS, Moore AR, Staudenmaier EK, Friedel RH, Paradis S. 2013. The class 4 semaphorin Sema4D promotes the rapid assembly of GABAergic synapses in rodent hippocampus. J Neurosci. 33:8961–8973.

Lee KH, Lee H, Yang CH, Ko JS, Park CH, Woo RS, Kim JY, Sun W, Kim JH, Ho WK, et al. 2015. Bidirectional signaling of neuregulin-2 mediates formation of GABAergic synapses and maturation of glutamatergic synapses in newborn granule cells of postnatal hippocampus. J Neurosci. 35:16479–16493.

Li Y, Zhou W, Li X, Zeng S, Liu M, Luo Q. 2007. Characterization of synchronized bursts in cultured hippocampal neuronal networks with learning training on microelectrode arrays. Biosens Bioelectron. 22:2976–2982.

Maffei A, Nataraj K, Nelson SB, Turrigiano GG. 2006. Potentiation of cortical inhibition by visual deprivation. Nature. 443:81–84.

Mailleux AA, Overholtzer M, Schmelzle T, Bouillet P, Strasser A, Brugge JS. 2007. BIM regulates apoptosis during mammary ductal morphogenesis, and its absence reveals alternative cell death mechanisms. Dev Cell. 12:221–234.

Marcantoni A, Carabelli V, Vandael DH, Comunanza V, Carbone E. 2009. PDE type-4 inhibition increases L-type Ca(2+) currents, action potential firing, and quantal size of exocytosis in mouse chromaffin cells. Pflugers Arch. 457:1093–1110.

Marcantoni A, Raymond EF, Carbone E, Marie H. 2014. Firing properties of entorhinal cortex neurons and early alterations in an Alzheimer's disease transgenic model. Pflugers Arch. 466:1437–1450.

Marín O. 2012. Interneuron dysfunction in psychiatric disorders. Nat Rev Neurosci. 13:107–120.

Maroof AM, Brown K, Shi SH, Studer L, Anderson SA. 2010. Prospective isolation of cortical interneuron precursors from mouse embryonic stem cells. J Neurosci. 30:4667–4675.

McBain CJ, Fisahn A. 2001. Interneurons unbound. Nat Rev Neurosci. 2:11–23.

Morello N, Plicato O, Piludu MA, Poddighe L, Serra MP, Quartu M, Corda MG, Giorgi O, Giustetto M. 2017. Effects of forced swimming stress on ERK and histone H3 phosphorylation in limbic areas of roman high- and low-avoidance rats. PLoS One. 12:e0170093.

Papale A, d'Isa R, Menna E, Cerovic M, Solari N, Hardingham N, Cambiaghi M, Cursi M, Barbacid M, Leocani L, et al. 2017. Severe intellectual disability and enhanced gamma-aminobutyric acidergic synaptogenesis in a novel model of rare RASopathies. Biol Psychiatry. 81:179–192.

Pyle JL, Kavalali ET, Piedras-Renteria ES, Tsien RW. 2000. Rapid reuse of readily releasable pool vesicles at hippocampal synapses. Neuron. 28:221–231.

Rapanelli M, Frick LR, Pittenger C. 2017. The role of interneurons in autism and tourette syndrome. Trends Neurosci. 40:397–407.

Repetto D, Camera P, Melani R, Morello N, Russo I, Calcagno E, Tomasoni R, Bianchi F, Berto G, Giustetto M, et al. 2014. p140Cap regulates memory and synaptic plasticity through Src-mediated and citron-N-mediated actin reorganization. J Neurosci. 34:1542–1553.

Sheng M, Hoogenraad CC. 2007. The postsynaptic architecture of excitatory synapses: a more quantitative view. Annu Rev Biochem. 76:823–847.

Shiri Z, Manseau F, Levesque M, Williams S, Avoli M. 2015. Interneuron activity leads to initiation of low-voltage fast-onset seizures. Ann Neurol. 77:541–546.

Somogyi P, Klausberger T. 2005. Defined types of cortical interneurone structure space and spike timing in the hippocampus. J Physiol. 562:9–26.

Succol F, Fiumelli H, Benfenati F, Cancedda L, Barberis A. 2012. Intracellular chloride concentration influences the GABA A receptor subunit composition. Nat Commun. 3: 710–738.

Tabuchi K, Blundell J, Etherton MR, Hammer RE, Liu X, Powell CM, Sudhof TC. 2007. A neuroligin-3 mutation implicated in autism increases inhibitory synaptic transmission in mice. Science. 318:71–76.

Taniguchi H, He M, Wu P, Kim S, Paik R, Sugino K, Kvitsiani D, Fu Y, Lu J, Lin Y, et al. 2011. A resource of Cre driver lines for genetic targeting of GABAergic neurons in cerebral cortex. Neuron. 71:995–1013.

Tatti R, Haley MS, Swanson OK, Tselha T, Maffei A. 2017. Review neurophysiology and regulation of the balance between excitation and inhibition in neocortical circuits. Biol Psychiatry. 81:821–831.

Tomasoni R, Repetto D, Morini R, Elia C, Gardoni F, Di Luca M, Turco E, Defilippi P, Matteoli M. 2013. SNAP-25 regulates spine formation through postsynaptic binding to p140Cap. Nat Commun. 4:2136.

Traynelis SF, Silver RA, Cull-Candy SG. 1993. Estimated conductance of glutamate receptor channels activated during EPSCs at the cerebellar mossy fiber-granule cell synapse. Neuron. 11:279–289.

Tricoire L, Pelkey KA, Erkkila BE, Jeffries BW, Yuan X, McBain CJ. 2011. A blueprint for the spatiotemporal origins of mouse hippocampal interneuron diversity. J Neurosci. 31: 10948–10970.

Trygve S, Moser EI, Gaute TE. 2007. From grid cells to place cells: a mathematical model. Hippocampus. 17:801–812.

Tyzio R, Cossart R, Khalilov I, Minlebaev M, Hubner CA, Represa A, Ben-Ari Y, Khazipov R. 2006. Maternal oxytocin triggers a transient inhibitory switch in GABA signaling in the fetal brain during delivery. Science. 314:1788–1792.

Tyzio R, Nardou R, Ferrari DC, Tsintsadze T, Shahrokhi A, Eftekhari S, Khalilov I, Tsintsadze V, Brouchoud C, Chazal G, et al. 2014. Oxytocin-mediated GABA inhibition during delivery attenuates autism pathogenesis in rodent offspring. Science. 343:675–679.

Vaghi V, Pennucci R, Talpo F, Corbetta S, Montinaro V, Barone C, Croci L, Spaiardi P, Consalez GG, Biella G, et al. 2014. Rac1 and Rac3 GTPases control synergistically the development of cortical and hippocampal GABAergic interneurons. Cereb Cortex. 24:1247–1258.

Wu Y, Liu D, Song Z. 2015. Neuronal networks and energy bursts in epilepsy. Neuroscience. 287:175–186.

Yekhlef L, Breschi GL, Lagostena L, Russo G, Taverna S. 2015. Selective activation of parvalbumin- or somatostatin-expressing interneurons triggers epileptic seizurelike activity in mouse medial entorhinal cortex. J Neurophysiol. 113: 1616–1630.

Yizhar O, Fenno LE, Prigge M, Schneider F, Davidson TJ, O'Shea DJ, Sohal VS, Goshen I, Finkelstein J, Paz JT, et al. 2011. Neocortical excitation/inhibition balance in information processing and social dysfunction. Nature. 477: 171–178.